Ernst Abbe Hochschule Jena
University of Applied Sciences

Faculty of Scientific Instrumentation

Internship Report

Design and Construction of PCBA Tester and Strain Analysis in PCB

Author:
Deepak Petchimuthu

Academic Supervisor (University):
Prof. Dr.-Ing. Ronny Gerbach, EAH Jena

Company Supervisor (Tesla):
Senior Engineer Vivek Muthu, Tesla Giga Factory Berlin

Date of Submission:
September 30, 2025

Declaration

I hereby declare that this report is the result of my own work carried out during my internship, except where otherwise stated. All sources of information used have been acknowledged appropriately.

Name: Deepak Petchimuthu
Date: September 30, 2025

Acknowledgements

I am grateful to the Manufacturing Test Engineering group at Tesla for mentorship and day-to-day guidance throughout this internship. I thank the fixture design mentors for their feedback on the clamshell architecture, probe-field layout, and planarity controls; the CAE/FEM team for support with model setup, mesh-convergence checks, and verification practices aligned with NAFEMS, the Reliability and Materials Lab for assistance with strain-gauge selection, surface preparation, and bonding in accordance with IPC-9704 and ASTM E1237 and the DAQ/LabVIEW engineers for help implementing real-time principal-strain computation and ICT/FCT sequencing.

I also acknowledge the Safety/CE compliance team for their guidance on EN ISO 13849-1, IEC 60204-1, and IEC 61010-1 the EOL Operations and Maintenance teams for integrating the fixture on the line, validating utilities and interlocks, and training operators; and the Model Shop and Procurement teams for rapid fabrication, component selection, and cost control.

Special thanks go to the production operators who supported pilot runs and provided practical feedback that improved ergonomics, usability, and cycle time. I am grateful to my academic supervisor for constructive reviews.

This work benefited from the use of National Instruments DAQ hardware and LabVIEW, standard off-the-shelf components. Any opinions and conclusions expressed here are my own and do not necessarily reflect the views of Tesla.

Abstract

The project details the design, construction, and validation of a production-ready functional test system for a new PCBA. The primary verification tasks were In-Circuit Test (ICT) and Functional Test (FCT). Accordingly, a dedicated ICT/FCT fixture was developed, integrating 200 spring-loaded test probes to exercise and verify electrical signals at designated test points. The mechatronic architecture employs low-rate probe engagement, thereby intrinsically limiting mechanical strain during automated test cycles. The system was engineered to meet CE requirements for safe deployment in a European production environment.

Strain analysis is performed using a three-element 45° rosette strain gauge. Data is acquired and processed by a high-speed National Instruments LabVIEW-based DAQ system to compute the maximum principal strain in real-time. To de-risk the design, a comprehensive Finite Element Method (FEM) analysis was conducted, following NAFEMS guidelines, identifying regions of peak stress for rosette placement.

Experimental validation, following procedures outlined in IPC-9704 and ASTM E1237, confirmed a maximum transient principal strain of $345\,\mu\varepsilon$. This maintains a safety margin of 13.7% below the industry-accepted IPC/JEDEC-9704 threshold of $400\,\mu\varepsilon$. The result is a dual-purpose system where electrical testing does not compromise long-term mechanical reliability, enabling high-volume production with enhanced quality assurance. Stran Testing implementation is for tester validation only.

Contents

Declaration

Acknowledgements

Abstract

List of Abbreviations

1 Introduction **1**
- 1.1 Project Background and Motivation 1
- 1.2 Internship Role and Scope 1
- 1.3 Structure of the Report 2

2 Literature Review **3**
- 2.1 Stress-Induced Solder Joint Failure (SISJF) 3
- 2.2 PCBA Testing Methodologies and Associated Risks 3
- 2.3 Strain Measurement and Analysis Techniques 3
- 2.4 Finite Element Method (FEM) in PCBA Reliability 3
- 2.5 Fixture Mechanics and Touchdown Control 4
- 2.6 Data Acquisition and Real-Time Computation 4
- 2.7 Safety and CE Compliance in Test Systems 4

3 System Architecture and Detailed Design **5**
- 3.1 Systematic Design Methodology (VDI 2221) 5
  - 3.1.1 Clarify and Define the Task 5
  - 3.1.2 Functional Structure 5
  - 3.1.3 Working Principles and Concept Generation 5
  - 3.1.4 Concept Evaluation and Selection 6
  - 3.1.5 Embodiment Design 6
  - 3.1.6 Detail Design 6
  - 3.1.7 Verification and Validation (V&V) 6
  - 3.1.8 Risk Management and CE Alignment 7
  - 3.1.9 Handover and Lifecycle 7
- 3.2 Mechanical Design 7
  - 3.2.1 Top Fixture Design: alignment, guidance, and touchdown 7
  - 3.2.2 Bottom Fixture Design: support, sensing, and guided closure . . . 8

3.2.3 Linear Actuation and Strain-Rate Control . . . 9
3.3 Gas Spring Design . . . 10
3.3.1 Safety Systems and CE Compliance . . . 10
3.4 Functional Workflow and Operation . . . 10
3.5 Verification: KPIs, FEM, and Test Evidence . . . 11

4 Modelling and Validation **14**
4.1 Process and Guidelines (NAFEMS-aligned) . . . 14
4.1.1 FEM Model Setup . . . 15
4.1.2 Top Fixture Plate (GAROLITE G10) — Probe Spring Retraction Analysis . . . 15
4.1.3 Tester Shaft and Baseplate — Gas-Spring and Top-Plate Loads . . . 16
4.1.4 Compliance, Safety Margins, and Governance . . . 17
4.1.5 Traceability and Coherence Map . . . 18
4.1.6 Reproducibility and Data Management . . . 18
4.1.7 Acceptance and Sign-off . . . 18

5 Experimental Strain Measurement Methodology **19**
5.1 Strain Gauge Theory and Piezoresistive Effect . . . 19
5.2 Placement of Strain Gauges on the PCBA . . . 19
5.3 PCB Layout Context and Test-Point Map . . . 20
5.4 Standardized Test Methodology . . . 21
5.5 Rosette Reduction and Principal Strains . . . 22
5.6 Instrumentation and Signal Conditioning . . . 23

6 LabVIEW Integration and Control System **25**
6.1 System Overview . . . 25
6.2 Hardware and Acquisition Parameters . . . 25
6.3 Software Architecture and Data Flow . . . 25
6.4 Calibration and Zeroing . . . 26
6.5 Computation and Acceptance . . . 26
6.6 Data Management and Traceability . . . 26
6.7 Scope and Assumptions . . . 26

7 Results, Discussion, and Validation **27**
7.1 Mechanical Design Assessment and Conformance with FEM . . . 27
7.1.1 Architecture and Design Intent . . . 27
7.1.2 Key Mechanical KPIs vs. Specifications . . . 27
7.1.3 Risk Closure and Mechanical Conclusion . . . 28
7.2 Data Set and Operating Conditions . . . 28

7.3 Descriptive Statistics of Mechanical Response 29
7.3.1 Peak principal strain 29
7.3.2 Transient characteristics 29
7.4 Process Capability vs. 400 $\mu\varepsilon$ 29
7.5 FEM–Experiment Correlation 29
7.6 Measurement Uncertainty and Gage R&R 30
7.6.1 Uncertainty budget for $\varepsilon_{1,\mathrm{peak}}$ 30
7.6.2 Gage R&R Summary 30

8 Conclusion **31**

References **32**

List of Figures

1 Datum and planarity controls with primary pin, slotted secondary pin, and probe-plate spacers. 8
2 Exploded view showing top plate, interface PCBA, probe plate and pogo field (incl. 3.00 A/8.00 A pins), static pushers, and standoffs 8
3 Bottom fixture: Delrin carrier plate, locating-pin bushings and UUT guide pins for kinematic seating; capacitive sensors for presence/seat check, static pushers for preload, rigid aluminium base 9
4 PCBA tester assembly in open postition. The top fixture descends on linear bearings; the PCBA is aligned on the carrier plate by tooling pins. 12
5 Exploded view: top plate/collar and handles, top fixture with linear bearings, moving plate, shafts, gas springs, bottom fixture, electromagnet, base plate, cable-chain holder, external dashpots with mechanical blocker, and transparent pinch protection. 12

6 Von Mises stress distribution on the top fixture plate (G10) under probe spring loads (limits and margins in Table 3). Peak ∼3.95 MPa. 16
7 Total displacement of the top fixture plate (G10) under probe spring loads (limits and margins in Table 3). Peak ∼0.0261 mm. 16
8 Von Mises stress on tester shaft and baseplate under gas-spring and top-plate loads (limits and margins in Table 3). Peak ∼8.52 MPa. 17
9 Total displacement of tester shaft and baseplate under operational loads (limits and margins in Table 3). Peak ∼0.005 51 mm. 17

10 Placement of a planar rosette at a BGA corner land pad. The centroid of the stacked rosette is positioned over the corner pad, and solder removal is minimised to what is strictly necessary to fit the rosette. (Adapted from project guidance.) 20
11 Bonded 0°/45°/90° strain-gauge rosette on the PCBA. Grids are aligned to the board axes and wired as three 3-wire quarter-bridge channel, soldered tabs and lead strain-relief loops are visible. Used during tester V&V to capture touchdown-transient principal strain per IPC/JEDEC-9704 and ASTM E1237. 20
12 PCB layout with test points, component placement, and strain-gauge locations used in this work. The map ensures coverage of high-risk regions and provides context for interpreting measured principal strains 21

13 Cycle-overlaid principal-strain histories at two rosette locations. Top row: Gauge 1 and Gauge 2 ε_1 (maximum principal). Bottom row: Gauge 1 and Gauge 2 ε_2 (minimum principal). The brief touchdown transient near $t \approx 0$ and small steady-state levels support the statistics and overshoot discussion in Sec. 7.3. 28

List of Tables

1 Representative parts and key information. 9
2 Mechanical KPI summary (specification vs. FEM and measured outcomes). 11

3 Design results and safety margins. 18
4 Design coherence map linking objectives, metrics, and FEM evidence. . . 18

5 Mechanical KPI summary (specification vs. FEM and measured outcomes). 27
6 Uncertainty budget (standard uncertainties) 30
7 Gage R&R summary. Standard deviations and percent of total variance. 30

List of Abbreviations

Abbreviation	Description
ADC	Analog-to-Digital Converter
ASTM	American Society for Testing and Materials
BGA	Ball Grid Array
BOM	Bill of Materials
CAD	Computer-Aided Design
CE	Conformité Européenne (European Conformity)
DAQ	Data Acquisition
DUT	Device Under Test
ECU	Electronic Control Unit
EMC	Electromagnetic Compatibility
FCT	Functional Circuit Test
FEM	Finite Element Method
FOS	Factor of Safety
GD&T	Geometric Dimensioning and Tolerancing
HSR	Hot-Spot Region
ICT	In-Circuit Test
IPC	Association Connecting Electronics Industries
JEDEC	Joint Electron Device Engineering Council
NAFEMS	National Agency for Finite Element Methods and Standards
PCBA	Printed Circuit Board Assembly
SISJF	Stress-Induced Solder Joint Failure
SPC	Statistical Process Control
TDMS	Technical Data Management Streaming
V&V	Verification and Validation

1 Introduction

1.1 Project Background and Motivation

The primary focus of this work is to achieve high-coverage In-Circuit Test (ICT) and Functional Test (FCT) using a purpose-built Test Bench that integrates 200 spring-loaded probes to stimulate and measure electrical signals at defined test points. To meet quality standards and protect long-term reliability, strain-gauge measurement is used once for tester/fixture validation rather than embedded in routine production. A three-element 45° rosette, coupled with high-speed data acquisition, quantifies principal strain during probe engagement, these measurements inform fixture design, touchdown control, and process limits to ensure mechanical loading remains within acceptable thresholds[5, 1, 19]. After this one-time validation, electrical testing proceeds without inline strain monitoring, operating within the established limits. This integrated approach delivers rigorous electrical verification while ensuring the test bench operates within validated mechanical constraints, enabling reliable and scalable production

1.2 Internship Role and Scope

The internship covered the full engineering cycle. I used VDI design methods to turn stakeholder needs into clear requirements and a complete design. I created a detailed 3D CAD model of a Test Bench for ICT and FCT, integrating 200 spring-loaded probes. I selected the mechanical and electrical parts, built the system, and added safety controls to meet CE standards[13, 14, 15].

Finite Element Method (FEM) analyses were performed on the test bench structure (baseplate, top plate, frame, and moving arms) to verify stiffness and deflection under combined probe and gas-spring loads. In line with NAFEMS best-practice guidelines for verification and validation in solid mechanics, the results informed plate thicknesses, ribbing, and fastener selections, and were corroborated by hand calculations and planarity measurements[12]. Newly developed PCBA, Strain-gauge target locations were then selected using IPC/JEDEC-9704 guidance. A three-element 45° rosette was bonded at the selected site, and maximum principal strain was computed in real time using an NI CompactDAQ and LabVIEW[19]. Experimental results confirmed that the peak strain remained below the IPC-9704 limit of $400\,\mu\varepsilon$[5]. Documentation was completed, users were trained, and the system was commissioned at the end-of-line (EOL) test station.

1.3 Structure of the Report

The report is organised as follows:

Literature and Standards: prior work on PCBA testing, ICT/FCT methods, applicable standards (Chapter 2).

Requirements and Design Method: stakeholder needs, derived requirements, VDI 2221/2206 process (Chapter 3, esp. Section 3.1).

Architecture, Detailed Design, and CE Compliance: system/fixture design, safety functions, CE evidence (Chapter 3, Sections 3.2 and 3.3.1).

Modelling and Simulation (FEM): PCBA strain model, fixture structural analysis, model V&V (Chapter 4).

Instrumentation, Software, and Test Procedures: strain gauges, NI DAQ/LabVIEW, ICT/FCT workflow (Chapters 5 and 6).

Results and Discussion: electrical coverage, strain results, interpretation, limitations (Chapter 7).

Conclusions: key findings and future work (Chapter 8).

2 Literature Review

2.1 Stress-Induced Solder Joint Failure (SISJF)

Test-induced board flexure and transient strain as a driver of SISJF have been recognised since the mid-2000s. IPC/JEDEC-9704 (2004; rev. A 2012) formalised strain-gauge methods and limits for printed boards subjected to handling and test[5]. Consortia studies on lead-free solders and NPL good-practice guides (2007; 2011) reported higher modulus and lower ductility for SAC alloys relative to Sn–Pb, increasing susceptibility to brittle cracking during flexure[18]. Crack initiation at the solder–pad interface during brief overloads, followed by growth under thermal and vibratory cycling, is consistently described across studies from the 2000s to the 2010s.

2.2 PCBA Testing Methodologies and Associated Risks

Industry and standards literature in the 2010s identify ICT as a major contributor to flex-induced strain due to dense probe fields and high actuation forces[17, 16]. FCT typically applies fewer probes and lower forces, yet poor fixture design or connector mating can still induce excessive flexure[18]. The present work focuses on an FCT application and shows that careful mechanical design and validation are essential to avoid damage.

2.3 Strain Measurement and Analysis Techniques

Bonded resistance strain gauges are widely used for PCBA strain measurement; IPC/JEDEC-9704 and ASTM E1237 codify gauge selection, installation, and data quality[5, 1]. Digital Image Correlation (DIC) offers full-field mapping and was comprehensively reviewed by Sutton et al. and Pan et al.[10, 11], but requires optical access and more complex logistics. Given production constraints, gauges were selected for in-situ validation of a production tester.

2.4 Finite Element Method (FEM) in PCBA Reliability

FEM has been applied to predict board displacement and strain without physical prototypes, commonly modelling PCBs with homogenised orthotropic FR-4/copper properties[18]. Best practice for model credibility follows formal V&V guidance for computational solid mechanics[12]. Although simplified, FEM is effective for locating relative hot-spots and comparing fixture strategies, with experiments used for validation.

2.5 Fixture Mechanics and Touchdown Control

Guidance highlights probe force, planarity, and touchdown velocity as primary drivers of flexure during ICT/FCT. Distributed supports, compliant nests, and damped actuation reduce the peak and rate of principal strain at engagement[16, 17]. Good-practice guides and JEDEC JESD22-B111 further emphasise controlled mating and low-insertion-force connectors to mitigate dynamic flexure[18, 20].

2.6 Data Acquisition and Real-Time Computation

Real-time principal-strain computation for short transients in production tests is well established and supported by application guidance for strain/bridge measurements with NI-DAQ and LabVIEW[19]. Best practice converges on 5.00 ksample/s to 20.0 ksample/s sampling with anti-alias filtering, synchronised pre/post-trigger windows, channel-wise conversion and planar-rosette reduction to $\varepsilon_1(t)$, peak detection on unfiltered data, and disciplined metadata/traceability to support SPC[19].

2.7 Safety and CE Compliance in Test Systems

Mechanical test equipment intended for production deployment in Europe is typically designed against harmonised standards. EN ISO 13849-1 addresses safety-related control systems; IEC 60204-1 covers the electrical equipment of machinery; and IEC 61010-1 applies to measurement and control equipment[13, 14, 15]. Industry guidance shows that integrating interlocks, guarded motion, and controlled actuation reduces both operator risk and strain-rate peaks during probe engagement.

3 System Architecture and Detailed Design

3.1 Systematic Design Methodology (VDI 2221)

Development followed VDI 2221 with explicit artefacts at each step to maintain traceability and enable objective verification. The process was tailored for a mechatronic ICT/FCT Test Bench intended for production under CE marking, with each decision recorded against measurable requirements and a defined verification method (analysis, test, or inspection).

3.1.1 Clarify and Define the Task

Stakeholder needs covered in-circuit test (ICT) and functional test (FCT) coverage across 200 test points, safe operation compliant with CE, end-of-line (EOL) integration, maintainability, cost, and cycle time. These needs were translated into a requirements list and a traceability matrix with acceptance criteria and verification routes. The primary project objective was the design, build, and CE-ready integration of a production ICT/FCT Tester, strain-gauge instrumentation was employed only during V&V to qualify the fixture mechanics and touchdown profile, not as a production measurement. The principal mechanical requirement was to limit maximum principal strain on the PCBA during probe engagement to $\leq 400\,\mu\varepsilon$ per IPC/JEDEC-9704[5]. System-level objectives required guarded motion with interlocks, a safety-rated E-stop that fails safe on power loss, and end-to-end traceability via serialization and calibration records. Constraints included utilities (power), floor-space envelope, acoustic noise, ESD control, and test access.

3.1.2 Functional Structure

The overall function, verifying the PCBA safely and repeatably was decomposed into aligning/locating the board, engaging probes with controlled force and velocity, providing ICT/FCT stimulus and measurement, acquiring transient strain, protecting the operator, logging data for traceability, and enabling diagnostics and safe recovery. A function-to-means mapping connected each subfunction to possible working principles and established clean mechanical, electrical, and information interfaces.

3.1.3 Working Principles and Concept Generation

Alternatives were developed using a morphological chart covering actuation (gas-spring, electric, manual), touchdown control (flow-controlled dashpots), support strategy (rigid pins, compliant nests, vacuum support), alignment features (guide pins with bushings, linear rails), probe planarity control (single rigid plate or floating plate), strain sensing (three-element 45° rosette gauges or digital image correlation), data acquisition platforms, and safety measures (interlocks, two-hand control, light curtains). First-order calculations

estimated the total probe force from vendor spring constants and target compression, predicted board deflection using simplified plate models, and sized damper settings to achieve a low-rate, repeatable touchdown. These bounds highlighted sensitive parameters prior to hardware commitment.

3.1.4 Concept Evaluation and Selection

Concepts were judged on PCBA-strain risk, electrical coverage, CE compliance, cycle time, cost, maintainability, and EOL risk using a Pugh matrix. A focused DFMEA addressed misalignment, over-travel, loss of damping, and mitigation strategies. The selected architecture is a gas-spring–actuated clamshell, distributed board supports, and a tight-flatness top probe plate.

3.1.5 Embodiment Design

Three-dimensional CAD defined hinge and arm geometry, upper and lower plates, the 200-point probe field, nests and supports, guards, and service access. FEM was used to tune support locations and to predict stress and strain under combined probe and clamp loads, details of correlation against measurements appear in Chapter 7 and Section 7.1. Damper settings were tuned to meet the desired touchdown velocity and force profile, with hard stops and over-travel protection incorporated. A stack-up and tolerance analysis set flatness and stiffness targets for plates, mounts, and probe bushings, verified on granite with dial indicators.

3.1.6 Detail Design

Detailed outputs comprised manufacturing drawings and a bill of materials, electrical and schematics, harnessing, and panel layout with I/O assignments. NI CompactDAQ with LabVIEW computes principal strain in real time from the rosette signals, sequences ICT/FCT, and logs serialized results[19]. The software architecture and data flow align with the operational sequence described in Section 3.4 and the validation evidence summarized in Section 3.5.

3.1.7 Verification and Validation (V&V)

Analytical checks confirmed forces, deflections, and factors of safety. FEM models were reviewed for mesh quality, convergence, and boundary-condition sensitivity. Bench measurements verified planarity, repeatability, and touchdown speed, while golden-unit ICT/FCT exercised the complete sequence. Strain tests with a bonded rosette captured the transient during probe engagement and verified that $\varepsilon_{1,\mathrm{peak}} < 400\,\mu\varepsilon$[5]; these data correlate to FEM predictions as discussed in Section 7.1 and Chapter 7. Final acceptance closed each requirement in the traceability matrix.

3.1.8 Risk Management and CE Alignment

Risks—mechanical and electrical—were mitigated via the hierarchy of controls. The design aligns with EN ISO 12100, IEC 60204-1 (electrical equipment), and IEC 61010-1 (measurement and control)[14, 15]. Interlocks, guards, an E-stop, and defined safe states were implemented and verified, with evidence recorded in the CE dossier referenced in Section 3.3.1.

3.1.9 Handover and Lifecycle

Handover encompassed work instructions, preventive maintenance plans, calibration procedures, and critical spares. The system was commissioned at EOL with operator and technician training. The design record includes the requirements and traceability matrices, function and morphology studies, selection rationale and DFMEA, sizing calculations, FEM results, CAD and drawings, schematics and BOM, software documentation, test protocols and results, and the CE technical file.

3.2 Mechanical Design

The fixture was designed to prioritize stiffness, precise guidance, and a shaped touchdown profile to limit both peak principal strain and its rate of change. Upper and lower plates use Aluminium 7075-T6 for high specific stiffness and strength, while precision components such as linear guides and tooling pins are hardened steel for wear resistance. The probe plates are machined from FR-4/G10 to combine electrical insulation with dimensional stability. Kinematics are fully constrained by the hinge and linear guidance, and the PCBA is supported on a distributed network of nests and pushers. The resulting architecture satisfies the strain limit, alignment repeatability, and fail-open safety objectives defined in Section 3.1.1, with verification by rosette measurements and FEM correlation.

3.2.1 Top Fixture Design: alignment, guidance, and touchdown

The top fixture aligns spring-loaded probes to PCBA pads and controls touchdown. The G10/FR-4 probe plate (thickness 8.00 mm) is specified to a flatness of ≤ 0.100 mm, and precision spacers establish clearance to adjacent components for uniform force distribution (Fig. 1). A primary locating pin serves as the datum, while a secondary slotted pin removes rotation without over-constraint; clearances are set at 1.27 mm to avoid clashes and to preserve creepage, clearance, and EMC through appropriate grounding of alignment features. Guidance is provided by hardened steel shafts with linear bearings to deliver low-tilt, near-pure Z-axis motion; bearing capacity is approximately 500 N per block with a misalignment tolerance of $\pm 0.005\,00$ mm. Gas springs assist with lift and balance, and adjustable external dashpots shape the final 0 mm to 2.00 mm of travel to suppress overshoot, a mechanical blocker allows damper bypass during setup and service. At dwell, electromagnets engage steel keepers to hold position without air, de-energizing on E-stop

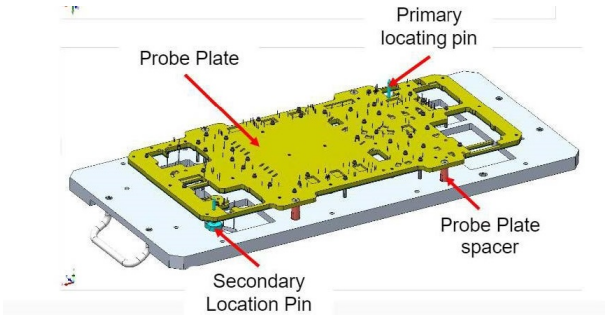

Figure 1: Datum and planarity controls with primary pin, slotted secondary pin, and probe-plate spacers.

or power loss so that gas springs return the assembly to a safe, open state. The interface PCBA routes signals to 3.00 A and 8.00 A probes and receptacles as required, and static pushers prevent local slip. FEM analysis supports the stiffness and planarity claims, with a maximum plate deflection of $\delta_{\max} \approx 0.0261$ mm under load, contributing to low dynamic overshoot. See chapter 7.1

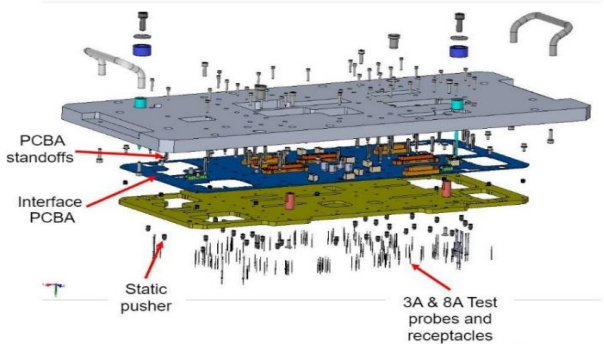

Figure 2: Exploded view showing top plate, interface PCBA, probe plate and pogo field (incl. 3.00 A/8.00 A pins), static pushers, and standoffs

3.2.2 Bottom Fixture Design: support, sensing, and guided closure

The bottom fixture aligns and secures the PCBA during test (Figs. 3. A Delrin carrier plate provides electrical insulation and tailored slots and standoffs to protect board surfaces while constraining position. Guided mating is achieved by precision bushings that accept the top fixture locating pins to ensure kinematic closure and planarity. Capacitive sensors (Keyence EX-V) confirm correct seating and orientation at a set gap of 0.100 cm to 0.300 cm with micrometre-level repeatability, providing analog outputs to the control system. Static pushers apply a controlled preload to stabilize the board during probe compression. The base plate, fabricated from 6061-T6 or 5052-H32 aluminium, provides high rigidity (6061-T6 $\sigma_{\text{UTS}} \approx 310$ MPa, $\sigma_y \approx 276$ MPa), minimizing vibration and maintaining geometry.

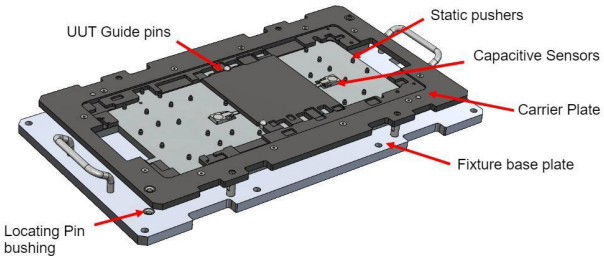

Figure 3: Bottom fixture: Delrin carrier plate, locating-pin bushings and UUT guide pins for kinematic seating; capacitive sensors for presence/seat check, static pushers for preload, rigid aluminium base

Table 1: Representative parts and key information.

Component	**Company**	**Key information**
Spring-loaded probes	Ingun	200 pieces; travel 3.00 mm; spring force 1.50 N at 1.50 mm; tip matched to pad type.
Probe plates	FR-4 (glass-epoxy)	Non-conductive; 8.00 mm thick; flatness $\leq$ 0.100 mm.
Hydraulic damper	ACE HB series	Adjustable damping; controls touchdown speed.
Linear guides	THK	Two rails with four blocks; maintains alignment and planarity.
Safety relay	Pilz PNOZ	E-stop logic; power removal (no air circuit).
Capacitive sensor	Keyence EX-V	Non-contact presence/position check; micrometre-level repeatability; set gap 0.100 mm to 0.300 mm; TTL/analog output to PLC.
Item frame (aluminium profile)	item MB 8, 45×45	Machine base; 45×45 profiles; corner brackets; levelling feet; mounting for guards/enclosures.

3.2.3 Linear Actuation and Strain-Rate Control

Primary motion is provided by gas springs that drive the Z-axis through the closing and opening strokes. Precision linear guides constrain motion to the Z-axis, preventing

lateral loads on pogo pins and the DUT. Electromagnet locks engage steel keepers to hold position at dwell/home, they de-energize on E-stop or power loss, after which the gas springs return the assembly to the safe open position. The magnets serve only as position holds and are not safety brakes.

3.3 Gas Spring Design

For Ingun GKS-100 probes, 200 pins at approximately 2.50 N each yield a total normal force near 500 N. The motion system is therefore sized so that the net available force during approach exceeds this value, with margin to cover friction, guidance losses, and preload from counterbalancing elements. In practice, two gas springs are selected so that their combined force at the operating position provides $\geq 1.5\times$ the aggregate probe force, allowing a lower approach rate and stable, repeatable engagement.

3.3.1 Safety Systems and CE Compliance

A risk assessment per ISO 12100 identified pinch points, stored mechanical energy in the gas springs, and electrical hazards. Mitigations include full guarding with transparent pinch protection, a safety-rated E-stop, interlocked access, and a two-hand start for the closing stroke. Electromagnet locks serve solely as position holds and are not safety brakes; consequently there is no compressed-air circuit to exhaust. On E-stop or power loss, the electromagnets de-energize and the gas springs bias the mechanism to the safe open position, with the hydraulic dampers passively dissipating motion. The design aligns with the Machinery Directive 2006/42/EC and the Low Voltage and EMC Directives, with supporting evidence compiled in the CE dossier referenced in Section 3.3.1 (and aligned to EN ISO 13849-1, IEC 60204-1, and IEC 61010-1)[13, 14, 15].

3.4 Functional Workflow and Operation

After initialization with device self-checks, DAQ configuration, and verified open position, the operator loads the PCBA, which is then verified by capacitive sensors for presence and orientation and close the handle for engagement. Test begins while the strain channels acquire a short baseline interval to zero the rosette. Touchdown is detected by either a force/position inflection or a slope threshold on the strain signal. A pre- and post-trigger window (50.0 ms and 250 ms, respectively) is recorded at a sampling rate of at least 10.0 kHz. The maximum principal strain $\varepsilon_1(t)$ is computed sample-by-sample and its absolute peak is tracked. When $|d\varepsilon_1/dt|$ falls below threshold for 20.0 ms to 50.0 ms, the system transitions to steady state, after which electrical ICT/FCT stimuli and measurements are applied.The system then retracts to open and logs time-stamped cycle data, including $\varepsilon_{1,\mathrm{peak}}$ and time of peak; full waveforms are archived for failures, while summaries are retained for trend analysis. This workflow underpins the evidence presented in Section 3.5.

3.5 Verification: KPIs, FEM, and Test Evidence

Measured peak principal strain was $\varepsilon_{1,\text{peak}} \approx 345\,\mu\varepsilon$ (limit $400\,\mu\varepsilon$); FEM predicted $\sim 360\,\mu\varepsilon$. Probe-plate deflection from FEM was $\delta_{\max} \approx 0.0261\,\text{mm}$ (target $\leq 0.0500\,\text{mm}$). See Chapter 4 for FEM modelling details and Chapter 7 for the broader results discussion.

Table 2: Mechanical KPI summary (specification vs. FEM and measured outcomes).

KPI	**Spec/Limit**	**FEM**	**Measured**	**Result / FoS**
PCBA peak strain $\varepsilon_{1,\text{peak}}$	$\leq 400\,\mu\varepsilon$	$\sim 360\,\mu\varepsilon$	$345\,\mu\varepsilon$	Pass (FoS $\approx 400/360 \approx 1.11$)
G10 plate von Mises stress $\sigma_{vM,\max}$	$\leq 248\,\text{MPa}$	$3.95\,\text{MPa}$	n/a	Pass (FoS ≈ 63)
G10 plate deflection $\delta_{\max}$	$\leq 0.0500\,\text{mm}$	$0.0261\,\text{mm}$	n/a	Pass (FoS ≈ 1.92)
Shaft stress (screening $0.5\,\sigma_y$)	$\leq 96.5\,\text{MPa}$	$8.52\,\text{MPa}$	n/a	Pass (FoS ≈ 11.3)
Shaft deflection $\delta_{\max}$	$\leq 0.0100\,\text{mm}$	$0.005\,51\,\text{mm}$	n/a	Pass (FoS ≈ 1.82)

Assembly Context (How to read)

Figures 4 and 5 provide assembly-level context. Figure 1 details the datum structure with the primary pin and the anti-rotation secondary pin and shows how spacers set probe-to-board height on the top fixture. Figure 2 expands the top assembly to illustrate how gas springs and linear bearings deliver balanced, vertical motion. Figure 3 identifies the sensors and pushers that confirm seating and stabilize the board, and shows the PCBA installed in the bottom fixture. The full energy and control path—including gas springs, electromagnets, and guards—can be seen in the exploded context of Figure 5, which supports the CE safety claims referenced in Section 3.3.1.

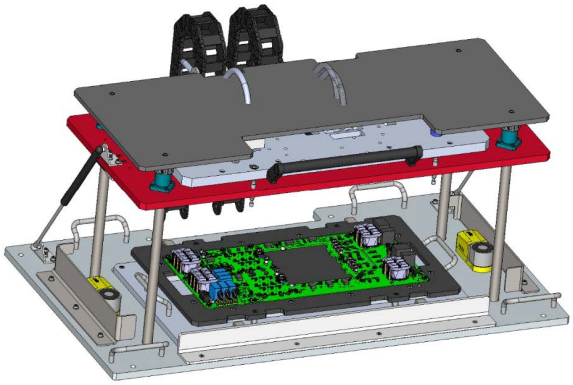

Figure 4: PCBA tester assembly in open postition. The top fixture descends on linear bearings; the PCBA is aligned on the carrier plate by tooling pins.

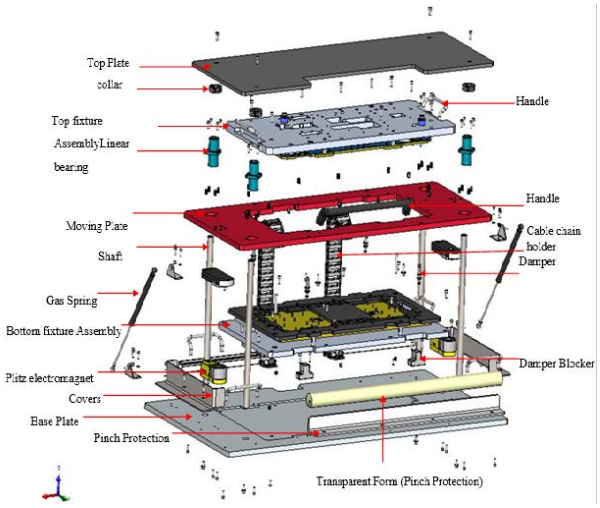

Figure 5: Exploded view: top plate/collar and handles, top fixture with linear bearings, moving plate, shafts, gas springs, bottom fixture, electromagnet, base plate, cable-chain holder, external dashpots with mechanical blocker, and transparent pinch protection.

Design Narrative

The design progression began with capturing requirements and constraints and defining verification methods and targets such as 200 test points measurements, $\varepsilon_{1,\text{peak}} \leq 400\,\mu\varepsilon$. Functions were decomposed and mapped to means using a morphological chart to explore alternatives. Actuation force was derived from the aggregate probe force, gas springs provided primary motion, and external hydraulic dampers shaped the final approach to control touchdown and strain rate. A kinematic location scheme with primary and secondary pins, together with hardened shafts and linear bearings, ensured planarity. Materials—Al 7075, FR-4/G10, hardened steel, and Delrin—were chosen to meet stiffness, insulation, and wear criteria. The fixture was modelled in CAD and analysed with FEM to tune supports and check deflection relative to the 0.0500 mm target. The BOM and schematics were produced in parallel with LabVIEW/DAQ implementation for real-time strain computation. Bench verification and golden-unit runs closed the loop, correlating strain to FEM and completing the traceability matrix.

4 Modelling and Validation

4.1 Process and Guidelines (NAFEMS-aligned)

The finite element method (FEM) predicts deformation and stress by splitting a complex part into many small elements. Supports and loads are applied, the linear system is solved for nodal displacements, and stresses are recovered and compared with allowables.

Define objectives and limits: Design-stage metrics focused on fixture integrity and alignment: top-plate (G10) stress below yield; top-plate planarity within 0.0500 mm; shaft stress below a 96.5 MPa screening limit (50% of 5052 yield), shaft straightness within 0.0100 mm.

Scope and simplification: Only load-bearing geometry was retained, cosmetic features were removed while preserving holes, contacts, and interfaces that influence load paths.

Materials and sources: Property values were recorded with datasheet or literature sources and tolerances to enable sensitivity studies.

Loads and boundary conditions: Physical forces (probe springs, clamps, gas springs) were mapped to equivalent pressures or nodal loads while preserving total force and first moments.

Meshing strategy: Target sizes and quality criteria were defined, local refinement was applied at probe seats, fasteners, bushings, and stiffness transitions.

Solver controls: Consistent SI units and a direct sparse solver were used, any non-default settings were documented.

Convergence plan: h-refinement was applied until changes in peak von Mises stress $\sigma_{\mathrm{vM,max}}$ and maximum displacement $\delta_{\max}$ fell below 5.00 %.

Design verification: Model probes, reaction tables, and contour plots were captured for review and traceability[12].

4.1.1 FEM Model Setup

Cleaned, de-featured CAD models were imported and meshed with second-order tetrahedra. Metallic support parts were modelled as Aluminium 7075-T6 except where noted. The moving top fixture plate was modelled as GAROLITE G10 (glass-fibre laminate). The tester shaft assembly was analysed separately in Aluminium 5052. Probe-field forces were represented at the probe seats, gas-spring forces were applied at their mounts. The base was fully fixed. Other interfaces followed the intended design constraints. All analyses used SI units with a direct sparse solver.

Materials and Constitutive Data

Aluminium 7075-T6: $E \approx 71.7\,\mathrm{GPa}$, $\nu = 0.33$, $\sigma_y \approx 503\,\mathrm{MPa}$.
GAROLITE G10 (screening): linear-elastic isotropic approximation; $\sigma_y \approx 248\,\mathrm{MPa}$.
Aluminium 5052 (shaft): $\sigma_y \approx 193\,\mathrm{MPa}$ (screening allowable 96.5 MPa).

Discretisation and Quality Metrics

Second-order tetrahedral (TET10) elements were used to capture curvature and reduce locking. Typical edge lengths were 0.600 mm near probe seats and bushings, 1.50 mm on plates, and 3.00 mm on brackets. Mesh quality thresholds: minimum Jacobian ≥ 0.45, aspect ratio ≤ 5, skewness ≤ 0.7.

Boundary Conditions and Loads

The base plate was fully constrained. The top plate was constrained at screw/spacer locations consistent with the design. Probe spring forces were applied at 148 seats with 0.710 N and at 12.0 seats with 3.00 N. Gas-spring forces of 178 N each and the top-plate weight of 187 N were applied at their mounts and directions. Load distributions preserved both resultant and first moments.

Governance and V&V (NAFEMS)

Verification included mesh refinement until $\Delta\sigma_{\mathrm{vM,max}}$ and $\Delta\delta_{\max} < 5.00\,\%$, global equilibrium within $\pm 1.00\,\%$, and plausibility checks of deformed shapes and stress flow[12].

4.1.2 Top Fixture Plate (GAROLITE G10) — Probe Spring Retraction Analysis

A design check was performed on the moving top plate made of GAROLITE G10. Spring forces at the probe seats represented the press-fitted test probes (148 at 0.710 N and 12.0 at 3.00 N). The plate was rigidly attached to the carriage at M4 45.0mm screw/spacer positions to the top aluminium plate.

With $\sigma_{y,\mathrm{G10}} \approx 248\,\mathrm{MPa}$, the analysis predicted $\sigma_{\mathrm{vM,max}} \approx 3.95\,\mathrm{MPa}$ and $\delta_{\max} \approx 0.0261\,\mathrm{mm}$ (see Table 3 for limits and safety margins).

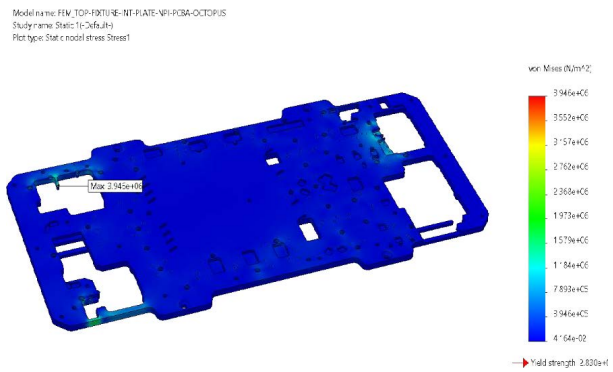

Figure 6: Von Mises stress distribution on the top fixture plate (G10) under probe spring loads (limits and margins in Table 3). Peak ∼3.95 MPa.

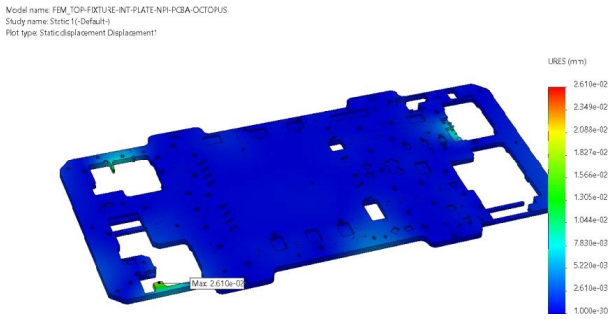

Figure 7: Total displacement of the top fixture plate (G10) under probe spring loads (limits and margins in Table 3). Peak ∼0.0261 mm.

Interpretation. Stress is far below $\sigma_{y,\mathrm{G10}}$, indicating negligible risk of damage. The small deflection supports uniform, repeatable contact.

4.1.3 Tester Shaft and Baseplate — Gas-Spring and Top-Plate Loads

A dedicated design check evaluated the shaft and structure response under the top-plate mass ($\approx 19.0\,\mathrm{kg}$, $187\,\mathrm{N}$) together with two gas springs set to $178\,\mathrm{N}$ each, the gas-spring load setting was explicitly verified and its influence assessed. Interfaces were modeled as bonded at the bushing–shaft and shaft–baseplate contacts. For Aluminium 5052, a screening allowable of 96.5 MPa was adopted for an alignment-focused assessment.

Predicted results were $\sigma_{\mathrm{vM,max}} \approx 8.52\,\mathrm{MPa}$ and $\delta_{\max} \approx 0.005\,51\,\mathrm{mm}$ (see Table 3 for limits and safety margins); both are within strength and straightness budgets.

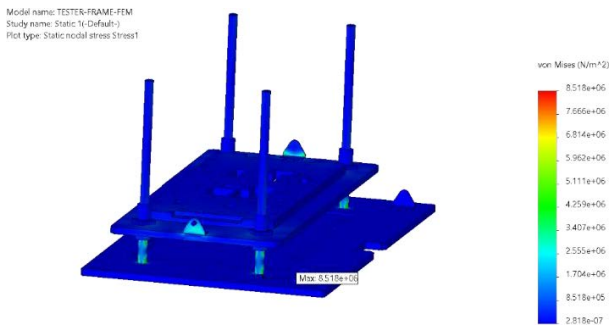

Figure 8: Von Mises stress on tester shaft and baseplate under gas-spring and top-plate loads (limits and margins in Table 3). Peak ∼8.52 MPa.

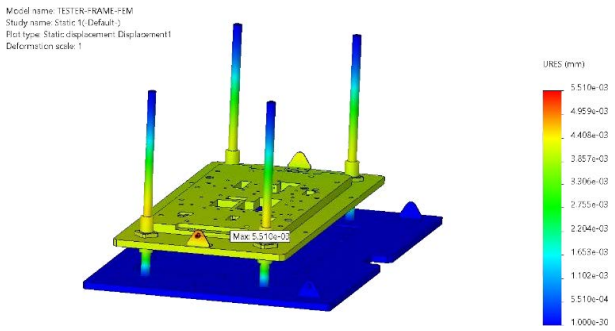

Figure 9: Total displacement of tester shaft and baseplate under operational loads (limits and margins in Table 3). Peak ∼0.005 51 mm.

Interpretation. Strength margin remains large even against the conservative $0.5\,\sigma_y$ screen; peak deflection is below the 0.0100 mm alignment budget.

4.1.4 Compliance, Safety Margins, and Governance

Definitions. Factor of Safety (FoS) $= \dfrac{\text{allowable}}{\text{actual}}$; Margin of Safety (MoS) $=$ FoS $- 1$ (positive indicates compliance).

Acceptance criteria.

- G10 plate strength: $\sigma_{\text{vM}} < 248$ MPa.
- G10 plate planarity: $\delta_{\max} \leq 0.0500$ mm.
- Shaft strength (screen): $\sigma_{\text{vM}} < 96.5$ MPa (50% of 5052 yield).
- Shaft alignment: $\delta_{\max} \leq 0.0100$ mm.

Computed margins.

- G10 stress: FoS $= 248/3.946 \approx 62.9$; MoS ≈ 61.9.
- G10 deflection: FoS $= 0.05/0.0261 \approx 1.92$; MoS ≈ 0.92.

- Shaft stress (screen): FoS = 96.5/8.518 ≈ 11.3; MoS ≈ 10.3. To yield: FoS = 193/8.518 ≈ 22.7.
- Shaft deflection: FoS = 0.01/0.00551 ≈ 1.82; MoS ≈ 0.82.

Table 3: Design results and safety margins.

Check	**Actual**	**Limit/Allow.**	**FoS**	**MoS**
G10 plate σ_{vM} (MPa)	3.946	248	62.9	61.9
G10 plate $\delta_{\max}$ (mm)	0.0261	0.05	1.92	0.92
Shaft σ_{vM} screen (MPa)	8.518	96.5	11.3	10.3
Shaft $\delta_{\max}$ (mm)	0.00551	0.01	1.82	0.82

4.1.5 Traceability and Coherence Map

Table 4: Design coherence map linking objectives, metrics, and FEM evidence.

Objective	**Metric/Limit**	**Design Evidence (FEM/Analytical)**	**Decision Rule**
Top plate integrity (G10)	$\sigma_{\mathrm{vM,max}} < 248\,\mathrm{MPa}$	$\sigma_{\mathrm{vM,max}} \approx 3.95\,\mathrm{MPa}$ under probe spring loads.	Accept if stress < yield.
Top plate planarity	$\delta_{\max} \leq 0.0500\,\mathrm{mm}$	$\delta_{\max} \approx 0.0261\,\mathrm{mm}$.	Accept if $\delta_{\max}$ within budget.
Shaft integrity (Al 5052)	$\sigma_{\mathrm{vM,max}} < 96.5\,\mathrm{MPa}$ (screen)	$\sigma_{\mathrm{vM,max}} \approx 8.52\,\mathrm{MPa}$ under gas-spring and weight loads.	Accept if stress < screening limit.
Shaft alignment	$\delta_{\max} \leq 0.0100\,\mathrm{mm}$	$\delta_{\max} \approx 0.005\,51\,\mathrm{mm}$.	Accept if $\delta_{\max}$ within budget.

4.1.6 Reproducibility and Data Management

Inputs (CAD hashes, material cards, mesh seeds, load/BC definitions, solver version) were placed under version control. Each analysis run has a unique ID with date/time, operator, and repository commit. Outputs (extrema summaries, reactions, deformed plots, exported CSVs) are archived. Any deviations from the nominal setup are listed.

4.1.7 Acceptance and Sign-off

Analysis is complete when convergence, the coherence map shows all objectives met, any residual differences are explained by sensitivity bounds or uncertainty and results are peer-reviewed and archived with full traceability.

5 Experimental Strain Measurement Methodology

A bonded metallic foil strain gauge is a thin serpentine metal grid on an insulating backing that is adhesively bonded to the test surface. When the surface deforms, the grid lengthens/shortens and its cross-section changes, producing a small change in electrical resistance. Exciting the gauge in a Wheatstone bridge and measuring the resulting millivolt-per-volt (mV/V) signal allows inference of surface strain. Typical foil gauges have $R_0 = 120\,\Omega$ or $350\,\Omega$ and gauge factor $G \approx 2$. For multi-directional measurements, three single gauges are arranged as a $0°/45°/90°$ rosette so principal strains can be computed.

5.1 Strain Gauge Theory and Piezoresistive Effect

For a gauge with nominal resistance R_0, the fractional resistance change is

$$\frac{\Delta R}{R_0} = G\,\varepsilon, \tag{5.1}$$

where G is the gauge factor and ε is the normal strain along the grid axis. For foil gauges used in board-level testing, $G \approx 2.0$–2.2 at room temperature. The gauge factor contains (i) a geometric term from lengthening/thinning of the grid (approximately $1 + 2\nu$, with ν the grid material's Poisson ratio) and (ii) a smaller piezoresistive term (strain-dependent resistivity).

5.2 Placement of Strain Gauges on the PCBA

Identifying critical areas for strain gauge placement is essential to assess the mechanical stress on the PCBA quantitatively. Consistent with IPC guidance (IPC-9701, 2022; IPC-9704, 2006), high-risk locations include corners and edges of ceramic packages, connector interfaces and panel/cutout boundaries, and regions prone to flexure near test-point clusters or stiffener transitions[5].

For corner-risk, a stacked rosette is centred on the corner land pad to align with principal strain directions. Where solder removal is necessary, it is limited strictly to the footprint required to seat the rosette. Alignment marks ensure the $0°/45°/90°$ grids are oriented with the local board axes. clearance from neighbouring pads and test points prevents strain bias from local stiffening. This strategy yields a defensible map of peak strains during the test event.

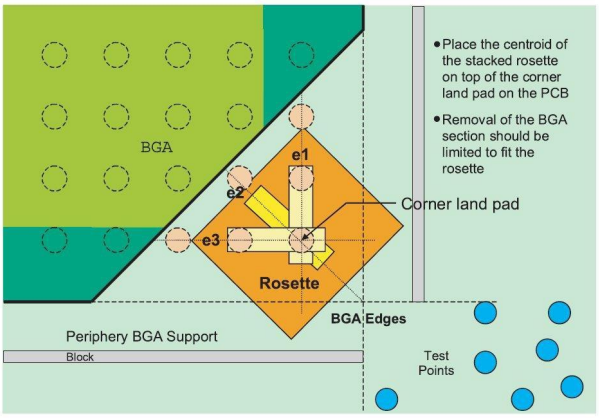

Figure 10: Placement of a planar rosette at a BGA corner land pad. The centroid of the stacked rosette is positioned over the corner pad, and solder removal is minimised to what is strictly necessary to fit the rosette. (Adapted from project guidance.)

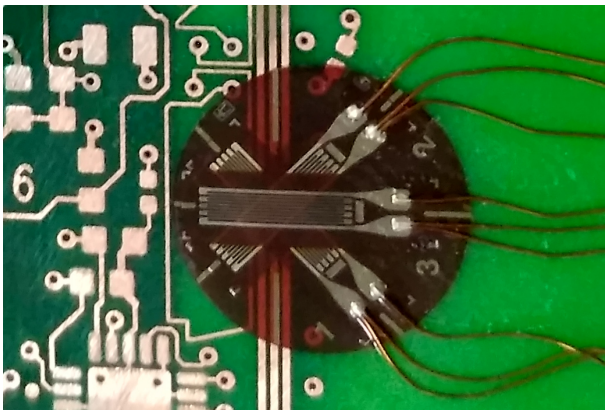

Figure 11: Bonded 0°/45°/90° strain-gauge rosette on the PCBA. Grids are aligned to the board axes and wired as three 3-wire quarter-bridge channel, soldered tabs and lead strain-relief loops are visible. Used during tester V&V to capture touchdown-transient principal strain per IPC/JEDEC-9704 and ASTM E1237.

5.3 PCB Layout Context and Test-Point Map

To verify that measured strains represent the global distribution across the assembly, gauge locations are chosen in the context of component placement and available test features. The layout overview (Fig. 12) shows major components, and test-point fields used for functional testing. Gauges were affixed following IPC-9704 alignment practices so that measured principal strains track the dominant flexure modes during approach, dwell, and release[5]. This approach confirmed that mechanical stresses remained within the 400 $\mu\varepsilon$ acceptance limit.

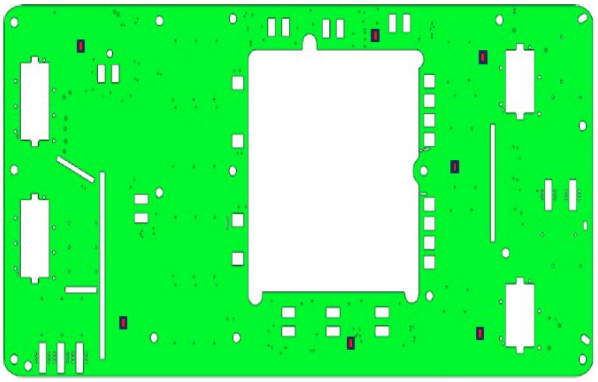

Figure 12: PCB layout with test points, component placement, and strain-gauge locations used in this work. The map ensures coverage of high-risk regions and provides context for interpreting measured principal strains

Outcome. By applying IPC-9701/9704 targeting and careful local installation, the test captured a comprehensive profile of strain distribution across the PCBA, verifying structural integrity within safe limits and guiding potential design or fixturing optimisations where needed.

5.4 Standardized Test Methodology

Complementary standards define where to measure and how to install/verify the instrumentation.

IPC/JEDEC-9704 (What/where to measure)

IPC/JEDEC-9704 (Printed Board Strain Gage Test Method) provides acceptance criteria and targeting guidance[5]:

Acceptance criterion:
Unless justified otherwise, the maximum principal surface strain at the event of interest must not exceed $400\,\mu\varepsilon$.

Target locations:
High-risk sites include BGA corners, large ceramic package edges, connector interfaces, cutouts, and stiffener boundaries. Gauges/rosettes are positioned to capture peak local strains induced by the operation (clamping, insertion/removal, handling).

Event consistency:
Fixturing/actuation should be repeatable with controlled engagement speed. In this work, actuation is manual with gas-spring return and dashpot-limited velocity. strain is recorded over approach, dwell, and release.

ASTM E1237 (How to install/verify)

ASTM E1237 (Guide for Installing Bonded Resistance Strain Gages) prescribes the installation and verification workflow[1]:

1. **Surface prep:** Clean per vendor guidance. Handle with gloves to avoid re-contamination.
2. **Layout/alignment:** Mark references so the 0° grid aligns with the board axis or known stress direction (target $\leq 1°$ angular error).
3. **Bonding:** Select adhesive for environment/timescale (cyanoacrylate for room-temperature dynamic events, epoxy for elevated temperature). Apply uniform pressure and follow the cure schedule.
4. **Wiring/strain-relief:** Prefer 3-wire quarter-bridge or 4-wire connections to minimize lead-wire error. Route twisted, shielded pairs, add service loops and secure leads so wire forces do not bias the measurement.
5. **Protection:** Apply a thin overcoat to guard against moisture and handling damage.
6. **Verification (shunt):** Insert a precision shunt resistor to create a known bridge output in mV/V and verify the DAQ scaling to an equivalent strain.

Uncertainty control - Dominant contributors include gauge-factor tolerance (typically $\pm 0.5\%$), alignment error, adhesive creep, temperature drift, and DAQ gain/linearity. Following the standards, using shunt calibration, and keeping procedures temperature-stable control these contributions[1, 19].

5.5 Rosette Reduction and Principal Strains

A 0°/45°/90° rosette measures the in-plane strain state. Denote the measured normal strains as ε_A (0°), ε_B (45°), and ε_C (90°). The principal strains are

$$\varepsilon_{1,2} = \frac{\varepsilon_A + \varepsilon_C}{2} \pm \sqrt{\left(\frac{\varepsilon_A - \varepsilon_C}{2}\right)^2 + \left(\frac{2\varepsilon_B - \varepsilon_A - \varepsilon_C}{2}\right)^2}, \tag{5.2}$$

and the principal direction (from the 0° grid toward ε_1) is

$$\theta_p = \tfrac{1}{2} \tan^{-1}\left(\frac{2\varepsilon_B - \varepsilon_A - \varepsilon_C}{\varepsilon_A - \varepsilon_C}\right). \tag{5.3}$$

Implementation guidance

Channel scaling: Convert each grid's bridge output (mV/V) to strain using the gauge factor and bridge configuration *before* rosette reduction. Apply transverse-sensitivity

correction.

Real-time computation: Compute $\varepsilon_1(t)$ and $\theta_p(t)$ sample-by-sample. A light, zero-phase low-pass filter (2nd–4th order), avoid filters that clip transient peaks.

Acceptance check: Compare $\max_t |\varepsilon_1(t)|$ to $400\,\mu\varepsilon$. Optionally require exceedance for $> 1.00\,\text{ms}$ to reject single-sample spikes[5].

5.6 Instrumentation and Signal Conditioning

A ratiometric Wheatstone bridge with a bridge-input DAQ (NI 9237) provides stable excitation, bridge completion, and low-noise digitization[19].

Bridge configuration and scaling

Bridge type:
Quarter-bridge (single active gauge with 3-wire compensation) is used for the three grids of the rosette (one channel per grid). Half-/full-bridge offers higher sensitivity and better temperature rejection when geometry allows.

Sensitivity (mV/V to strain):
For small strains,

$$\frac{V_{\text{out}}}{V_{\text{exc}}} \approx \begin{cases} \frac{G}{4}\,\varepsilon, & \text{quarter-bridge (1 active)}, \\ \frac{G}{2}\,\varepsilon, & \text{half-bridge (2 active)}, \\ G\,\varepsilon, & \text{full-bridge (4 active)}. \end{cases} \tag{5.4}$$

Therefore, for a quarter-bridge,

$$\varepsilon \approx \frac{4}{G}\,\frac{V_{\text{out}}}{V_{\text{exc}}}. \tag{5.5}$$

Bridge DAQs typically scale mV/V to strain directly when G and bridge type are specified, shunt calibration validates the end-to-end scale *in situ*[19].

Selected hardware:
NI 9237 with internal bridge completion ($120\,\Omega/350\,\Omega$), stable excitation, and direct mV/V acquisition. Three quarter-bridge, 3-wire channels are used—one per 0°, 45°, 90° grid[19].

Data Reduction and Reporting

For each test event, report:

1) Time histories of $\varepsilon_A(t)$, $\varepsilon_B(t)$, $\varepsilon_C(t)$, and $\varepsilon_1(t)$, including sample rate and filter settings.

2) Peak absolute principal strain and pass/fail against $400\,\mu\varepsilon$.

3) Installation details: gauge type, adhesive and cure schedule, alignment notes/photos.

4) Calibration traceability: shunt resistor value/tolerance, pre/post calibration results, DAQ configuration.

Rationale- IPC/JEDEC-9704 ensures measurements are taken at the correct locations with a defensible 400 $\mu\varepsilon$ limit tied to component/joint risk, while ASTM E1237 establishes installation and verification practices[5, 1]. Together with real-time rosette reduction, this provides repeatable, traceable strain measurements that a reviewer can audit and reproduce.

6 LabVIEW Integration and Control System

LabVIEW-based strain acquisition and analysis system implemented on NI Compact DAQ for planar rosette measurements. The application reads three single-element foil gauges at 0°, 45°, and 90°, computes principal strain in real time, visualises the results, and logs data for traceability. All fixture actuation functions (electromagnet holding, and functional electrical test sequencing) are out of scope and not controlled or interlocked by LabVIEW in this validation-only implementation[19].

6.1 System Overview

Three single-element foil gauges form a planar rosette and are wired as quarter-bridge, three-wire circuits to minimize lead-wire error with straightforward PCB implementation. Acquisition uses an NI 9237 (four channels, 24-bit, bridge input) providing excitation and bridge completion. Channels AI0, AI1, and AI2 are assigned to the 0°, 45°, and 90° grids, respectively; AI3 remains available for a dummy element or future expansion. Per-channel gauge factor G and nominal resistance R_0 are specified in software to ensure correct scaling[19].

6.2 Hardware and Acquisition Parameters

Acquisition parameters balance fidelity and data volume. Excitation is set between 2.5 and 5 V, selecting the lowest value that yields a stable baseline to limit self-heating. Sampling between 500 and 2000 Hz captures approach, dwell, and release transients without excessive file sizes. NI-DAQmx is configured for quarter-bridge, three-wire operation (350 Ω, Quarter Bridge II) with per-channel G and R_0. A light zero-phase low-pass filter may be applied for on-screen readability; the filter is display-only[19].

6.3 Software Architecture and Data Flow

The application follows a deterministic state-machine framework to ensure reproducibility, modularity, and clarity:

Initialization: Configure NI 9237 tasks (bridge mode, G, R_0) and perform shunt calibration.

Zero/Idle: With the DUT unloaded, execute electronic zero and verify stable baselines.

Awaiting Load: Monitor readiness signals and operator input.

Acquisition: Stream mV/V from AI0–AI2 and convert to ε_A, ε_B, and ε_C.

Strain Reduction: Compute maximum principal strain $\varepsilon_1(t)$ sample-by-sample and track the running absolute peak.

Decision & Logging: Compare $\varepsilon_1^{\text{peak}}$ to the acceptance limit and record results.

The graphical user interface presents live plots of $\varepsilon_A(t)$, $\varepsilon_B(t)$, $\varepsilon_C(t)$, and $\varepsilon_1(t)$, a numeric peak display, a pass/fail indicator, and operator controls (initialize, zero, start, stop).

6.4 Calibration and Zeroing

Initialise Per-channel precision shunt calibration verifies the expected mV/V response and equivalent strain, scaling is adjusted if necessary. With no load applied, an electronic zero removes residual offsets before testing. Baseline drift is checked with excitation enabled, if observed, excitation is reduced or warm-up time extended to ensure stability[19].

6.5 Computation and Acceptance

Principal strain $\varepsilon_1(t)$ is computed from the three rosette channels using the standard planar rosette transformation. Following IPC/JEDEC-9704 guidance, acceptance is defined as

$$\max_t \left|\varepsilon_1(t)\right| \leq 400\,\mu\varepsilon.$$

Peak detection operates on *unfiltered* data to avoid distortion of extremes; any display filtering is strictly zero-phase[5].

6.6 Data Management and Traceability

Each record includes the time series $\varepsilon_A(t)$, $\varepsilon_B(t)$, $\varepsilon_C(t)$, and $\varepsilon_1(t)$, with optional raw mV/V. Metadata capture gauge type, G, R_0, bridge configuration, sampling rate, display-filter settings, operator and DUT identifiers, and a summary containing $\varepsilon_1^{\text{peak}}$ with a pass/fail flag relative to the $400\,\mu\varepsilon$ criterion. Data are written to TDMS or CSV for downstream analysis and archival[19].

6.7 Scope and Assumptions

This implementation is limited to strain acquisition, real-time principal-strain computation, visualization, and logging. Correct results depend on proper gauge installation and wiring per ASTM E1237 and an appropriate test definition consistent with IPC/JEDEC-9704[1, 5]. Under these conditions, the system provides reliable, real-time assessment of principal strain with robust traceability suitable for production validation.

7 Results, Discussion, and Validation

The measured mechanical response of the PCBA during probe engagement, compares it with FEM predictions, quantifies measurement uncertainty, and evaluates process capability against the 400 µε acceptance limit (IPC/JEDEC-9704)[5]. Unless noted otherwise, strain refers to the maximum principal strain $\varepsilon_{1,\text{peak}}$ computed in real time from a 0°/45°/90° rosette.

7.1 Mechanical Design Assessment and Conformance with FEM

This section links the fixture architecture to FEM and measurement results, showing that strength, stiffness, planarity, and PCBA-strain objectives are met with margin.

7.1.1 Architecture and Design Intent

The fixture employs precision linear guidance to preserve planarity, a GAROLITE G10 moving probe plate for electrical insulation and dimensional stability, gas springs for counterbalance, external dashpots for a damped touchdown, an electromagnet for dwell holding, and a stiff base with distributed PCB supports. The design targets were: $\varepsilon_{1,\text{peak}} \leq 400\,\mu\varepsilon$ on the PCBA, probe-plate deflection $\delta_{\text{plate}} \leq 0.0500\,\text{mm}$ to maintain uniform contact, shaft/base stresses well below allowables with $\delta_{\text{shaft}} \leq 0.0100\,\text{mm}$ to preserve alignment.

7.1.2 Key Mechanical KPIs vs. Specifications

Table 5: Mechanical KPI summary (specification vs. FEM and measured outcomes).

KPI	Spec/Limit	FEM	Measured	Result / FoS
PCBA peak strain $\varepsilon_{1,\text{peak}}$	$\leq 400\,\mu\varepsilon$	$\sim 360\,\mu\varepsilon$	$345\,\mu\varepsilon$	Pass (FoS ≈ 1.11)
G10 plate stress $\sigma_{\text{vM,max}}$	$\leq 248\,\text{MPa}$	$3.95\,\text{MPa}$	n/a	FoS ≈ 63
G10 plate deflection δ_{max}	$\leq 0.0500\,\text{mm}$	$0.0261\,\text{mm}$	n/a	FoS ≈ 1.92
Shaft stress (screening $0.5\,\sigma_y$)	$\leq 96.5\,\text{MPa}$	$8.52\,\text{MPa}$	n/a	FoS ≈ 11.3
Shaft deflection δ_{max}	$\leq 0.0100\,\text{mm}$	$0.005\,51\,\text{mm}$	n/a	FoS ≈ 1.82

The G10 plate is lightly stressed and sufficiently stiff, with deflection at roughly half of the 0.0500 mm planarity budget. Shaft/base stresses are well below conservative allowables, and the predicted shaft deflection below 10.0 µm preserves guidance alignment. PCBA strain meets the 400 µε criterion with headroom, measurement agrees with FEM to approximately 4.00 % Less from the Limit.

7.1.3 Risk Closure and Mechanical Conclusion

The risk of high engagement strain is controlled (capability $C_{pk}^{+} = 1.86$). Loss of planarity is bounded by field checks. Structural yielding has large factors of safety on G10 and aluminium parts. Overall, the mechanical architecture is consistent with FEM and experiment: strength and stiffness margins are large, planarity stays within budget, and PCBA strain remains comfortably below $400\,\mu\varepsilon$ with low overshoot. The design is validated for end-of-line use under the documented conditions.

7.2 Data Set and Operating Conditions

Ten production-representative boards were each cycled five times for a total of $N = 50$ cycles. The fixture operated in damped descent mode with gas springs active, using standard supports and the production probe field. Strain acquisition was performed at 10.0 kHz per rosette channel with 50.0 ms pre-trigger and 250 ms post-trigger windows, peak tracking used unfiltered data. The environment was controlled at $25.0 \pm 1.00\,^{\circ}\mathrm{C}$ and 35.0 % to 45.0 % RH. Gauges followed IPC/JEDEC-9704 targeting, ASTM E1237 surface preparation and shunt verification, with $G = 2.0$ quarter-bridge three-wire completion[5, 1].

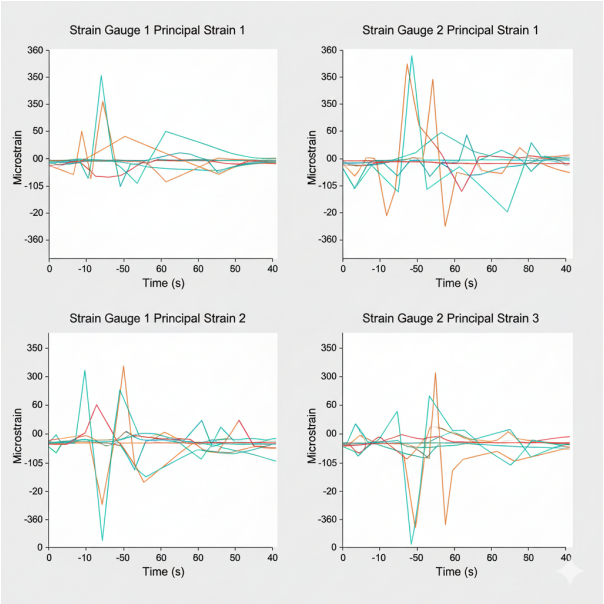

Figure 13: Cycle-overlaid principal-strain histories at two rosette locations. Top row: Gauge 1 and Gauge 2 ε_1 (maximum principal). Bottom row: Gauge 1 and Gauge 2 ε_2 (minimum principal). The brief touchdown transient near $t \approx 0$ and small steady-state levels support the statistics and overshoot discussion in Sec. 7.3.

7.3 Descriptive Statistics of Mechanical Response

7.3.1 Peak principal strain

We ran $N = 50$ cycles. The average peak principal strain was

$$\bar{\varepsilon}_{1,\mathrm{peak}} = 345\,\mu\varepsilon, \qquad s = 9.80\,\mu\varepsilon. \tag{7.1}$$

Simple take: typical peaks are around $345\,\mu\varepsilon$ with a small cycle-to-cycle spread.

A two-sided 95.0 % confidence interval for the true average is

$$\bar{\varepsilon}_{1,\mathrm{peak}} \pm t_{0.975,\,49}\,\frac{s}{\sqrt{N}} = 345\,\mu\varepsilon \pm 2.80\,\mu\varepsilon \;\Rightarrow\; \Big[342\,\mu\varepsilon,\ 348\,\mu\varepsilon\Big]. \tag{7.2}$$

Meaning: the long-run average is very likely between 342 and $348\,\mu\varepsilon$.

Assuming a normal (bell-curve) distribution, the upper percentiles are

$$\hat{P}_{95} \approx \bar{\varepsilon}_{1,\mathrm{peak}} + 1.645\,s = 361\,\mu\varepsilon, \qquad \hat{P}_{99.9} \approx \bar{\varepsilon}_{1,\mathrm{peak}} + 3.090\,s = 376\,\mu\varepsilon. \tag{7.3}$$

Meaning: even rare peaks stay well below the $400\,\mu\varepsilon$ limit.

7.3.2 Transient characteristics

From the contact trigger, the average time to reach the peak was $t_{\mathrm{peak}} = 0.205\,\mathrm{s}$ with a spread of $s = 0.0240\,\mathrm{s}$. The steady level (average over the last 50.0 ms) was $\varepsilon_{1,\mathrm{ss}} \approx 322\,\mu\varepsilon$. The overshoot is

$$M_p = \frac{\varepsilon_{1,\mathrm{peak}} - \varepsilon_{1,\mathrm{ss}}}{\varepsilon_{1,\mathrm{ss}}} \approx 7.20\,\%\ (\pm 2.00\,\%), \tag{7.4}$$

which shows the touchdown is well damped. *Meaning:* only a small, well-controlled bump above the steady level.

7.4 Process Capability vs. $400\,\mu\varepsilon$

The design's upper specification limit (USL) is $400\,\mu\varepsilon$. With no lower limit, the one-sided capability index is

$$C_{pk}^{+} = \frac{\mathrm{USL} - \mu}{3\sigma} = \frac{400\,\mu\varepsilon - 345\,\mu\varepsilon}{3 \times 9.80\,\mu\varepsilon} \approx 1.86. \tag{7.5}$$

Meaning: C_{pk}^{+} above 1.33 is usually considered very capable; 1.86 gives comfortable margin.

7.5 FEM–Experiment Correlation

The FEM model predicted $\varepsilon_{1,\mathrm{FEM}} \approx 360\,\mu\varepsilon$ at the gauged corner. The measured mean was $345\,\mu\varepsilon$.

7.6 Measurement Uncertainty and Gage R&R

7.6.1 Uncertainty budget for $\varepsilon_{1,\mathbf{peak}}$

Table 6 lists the main contributors around $350\,\mu\varepsilon$. We combine them by root-sum-square (RSS) to get the total standard uncertainty u_c, then use $U = k\,u_c$ with $k = 2$.

Table 6: Uncertainty budget (standard uncertainties)

Source	**Model**	**Std. unc. ($\mu\varepsilon$)**
Gauge factor ($\pm 0.5\%$, rectangular)	$0.005 \times 350/\sqrt{3}$	1.00
Amplifier gain ($\pm 0.2\%$, rectangular)	$0.002 \times 350/\sqrt{3}$	0.400
Rosette orientation ($\pm 2°$, rectangular)	$0.012 \times 350/\sqrt{3}$	2.40
Baseline/zero repeatability (Type A)	empirical	3.00
ADC noise (Type A)	RMS	2.00
Thermal drift ($1.00\,\mu\varepsilon/°\mathrm{C}$, $\pm 1.00\,°\mathrm{C}$, triangular)	$1/\sqrt{6}$	0.400
Combined (RSS) u_c		**4.48**
Expanded ($k = 2$) U		**8.96**

7.6.2 Gage R&R Summary

Table 7 provides a summary of the Gage R&R (Repeatability and Reproducibility) study, which assesses the capability of the measurement system relative to the total process variation.

Table 7: Gage R&R summary. Standard deviations and percent of total variance.

Component	**Std. dev. ($\mu\varepsilon$)**	**% of total variance**
Total variation (σ_{total})	9.80	100
Gage (σ_{gage})	1.80	3.40
Part-to-part (σ_{part})	9.60	96.6
$\text{ndc} = 1.41\,\sigma_{\text{part}}/\sigma_{\text{gage}} = 7.5$ (acceptable ≥ 5)		

*T*he measurement system is acceptable. The variation from the gage (3.4%) is a very small share of the total spread, and the ‘ndc‘ of 7.5 is well above the typical acceptance threshold of 5. This indicates the system can reliably distinguish between different parts.

8 Conclusion

A production functional tester and strain-measurement workflow were designed, implemented, and validated to combine functional verification with intrinsically controlled mechanical loading. Across repeated cycles, the peak principal strain at the critical corner averaged 345 $\mu\varepsilon$, providing a 13.7 % margin to the 400 $\mu\varepsilon$ guideline[5]. Finite-element predictions (360 $\mu\varepsilon$) agreed within about 5.00 %, and fixture stresses and deflections showed large safety factors, confirming a robust mechanical design. The measurement system was configured to be traceable and capable, and the overall process demonstrated strong capability for production use (one-sided $C_{pk} \approx 1.86$). The tester is therefore ready for end-of-line deployment under the documented conditions.

References

[1] ASTM International. ASTM E1237-17: Standard Guide for Installing Bonded Resistance Strain Gages. West Conshohocken, PA, 2017.

[2] Bathe, K.J. *Finite Element Procedures*. Prentice Hall, 1996.

[3] Clech, J.P. Board-level solder joint reliability of IC packages subjected to mechanical drop and bending. *APEX 2007 Proceedings*, 2007.

[4] Dally, J.W., & Riley, W.F. *Experimental Stress Analysis*, 4th ed. McGraw-Hill, 2005.

[5] IPC/JEDEC. IPC/JEDEC-9704A: Printed Board Strain Gage Test Guideline. 2012.

[6] Montgomery, D.C. *Introduction to Statistical Quality Control*, 8th ed. Wiley, 2020.

[7] NAFEMS. *How to Get Started with Finite Element Analysis*. 2020.

[8] Pitarresi, J., et al. A review and evaluation of printed circuit board material property models. *Proc. 9th International Congress on Experimental Mechanics*, 2004.

[9] Song, M. FEM and experimental analysis of PCB strain distribution. *Microelectronics Reliability*, 2015.

[10] Sutton, M. A., Orteu, J.-J., & Schreier, H. W. *Image Correlation for Shape, Motion and Deformation Measurements: Basic Concepts, Theory and Applications*. Springer, 2009.

[11] Pan, B., Qian, K., Xie, H., & Asundi, A. Two-dimensional digital image correlation for in-plane displacement and strain measurement: a review. *Measurement Science and Technology*, 20 (2009), 062001.

[12] ASME. V&V 10-2012: Guide for Verification and Validation in Computational Solid Mechanics. American Society of Mechanical Engineers, 2012.

[13] ISO. EN ISO 13849-1: Safety of machinery — Safety-related parts of control systems — Part 1: General principles for design. 2015.

[14] IEC. IEC 60204-1: Safety of machinery — Electrical equipment of machines — Part 1: General requirements. 2018.

[15] IEC. IEC 61010-1: Safety requirements for electrical equipment for measurement, control, and laboratory use — Part 1: General requirements. 2010.

[16] Keysight Technologies. Managing PCB Strain During In-Circuit Test (ICT) (Application Note). 2014–2018.

[17] Teradyne. Reducing PCB Flexure in ICT Fixtures (White Paper). 2011; 2016.

[18] National Physical Laboratory (NPL). Printed Circuit Board Strain Measurement and Control (Good Practice Guide). 2007; updated 2011.

[19] National Instruments. Strain/Bridge Measurements with NI-DAQ and LabVIEW (How-To Guide / Application Note). 2012; updated 2019.

[20] JEDEC Solid State Technology Association. JESD22-B111: Board Level Drop Test Method of Components for Handheld Electronic Products. 2017.

[21] VDI. VDI 2221: Systematic approach to the development and design of technical systems and products. 1993.

[22] Syed, A. Reliability and data correlation of lead free solder joints. *Proc. 56th Electronic Components and Technology Conference*, 2006.

[23] Vichare, N., et al. In-situ monitoring of mechanical stresses in a printed circuit board during manufacturing and testing. *Proc. 54th ECTC*, 2004.